

Dependence of the Macroscopic Quantum Tunneling Rate on Josephson Junction Area

Christoph Kaiser,¹ Roland Schäfer,^{2,3,*} and Michael Siegel^{1,3}

¹*Institut für Mikro- und Nanoelektronische Systeme,
Karlsruher Institut für Technologie, Hertzstraße 16, D-76187 Karlsruhe, Germany*

²*Institut für Festkörperphysik, Karlsruher Institut für Technologie,
Hermann-von-Helmholtz-Platz 1, D-76344 Eggenstein-Leopoldshafen, Germany*

³*Center for Functional Nanostructures, Karlsruher Institut für Technologie,
Wolfgang-Gaede-Straße 1a, D-76128 Karlsruhe, Germany*

(Dated: November 19, 2010)

We have carried out systematic Macroscopic Quantum Tunneling (MQT) experiments on Nb/Al-AlO_x/Nb Josephson junctions (JJs) of different areas. Employing on-chip lumped element inductors, we have decoupled the JJs from their environmental line impedances at the frequencies relevant for MQT. This allowed us to study the crossover from the thermal to the quantum regime in the low damping limit. A clear reduction of the crossover temperature with increasing JJ size is observed and found to be in excellent agreement with theory. All junctions were realized on the same chip and were thoroughly characterized before the quantum measurements.

PACS numbers: 74.50.+r, 85.25.Cp, 74.78.Na

I. INTRODUCTION

Since the gauge-invariant phase over a Josephson junction (JJ) φ is a macroscopic variable, circuits containing JJs have been used as model systems for the investigation of quantum dynamics on a macroscopic scale. This research has recently led to the development of different types of superconducting quantum bits^{1–5}, which are promising candidates for the implementation of quantum computers. The starting point of this field was the observation of Macroscopic Quantum Tunneling (MQT) in Josephson junctions in the 1980s^{6,7}. In such experiments, the macroscopic variable φ is trapped in the local minimum of a tilted washboard potential, before it tunnels through the potential barrier and starts rolling down the sloped potential. Since this running state is equivalent to the occurrence of a voltage drop over the junction, such tunneling events can be experimentally detected. MQT—often referred to as secondary quantum effect—is the manifestation of the quantum mechanical behavior of a single macroscopic degree of freedom in a complex quantum system. Furthermore, it is the main effect on which all quantum devices operated in the phase regime (such as phase qubits and flux qubits) are based. Consequently, the detailed understanding of MQT is not only interesting by itself, but also important for current research on superconducting qubits operated in the phase regime. In this article, we report on a systematic experimental study of the dependence of the macroscopic quantum tunneling rate on the Josephson junction area, which to our knowledge has never been performed before. As usual^{6–8}, we measure the rate at which the escape of φ out of the local minimum of the washboard potential occurs as a function of temperature. At high temperatures, the escape is driven by thermal fluctuation over the barrier while it is dominated by tunneling at low temperatures. This leads to a characteristic saturation of the temperature dependent tunneling rate be-

low a crossover temperature T_{cr} , which is the hallmark of MQT. The rates above and below crossover are affected by the dissipative coupling to the environment of the JJ, which is commonly accounted for by a quality factor Q in theoretical descriptions. A major goal of the presented study was to keep the influence of Q on the rate constant while varying the junction area, so that a change in the observed escape rates could be clearly assigned to the changed JJ size. For this purpose, we work in the underdamped regime of large Q , which is only possible if the JJ is to some extent decoupled from its low-impedance environment (i.e. the transmission line leading to the JJ). We achieve this by employing on-chip lumped element inductors.

This article is organized as follows: First, the physical model of MQT is discussed and the theoretical expectations for varying junction size are given. Second, the procedure and setup of measurement are described. Afterwards, the investigated Josephson junctions are characterized carefully, and finally, the results of the MQT measurements are presented and discussed.

II. MODEL AND MACROSCOPIC QUANTUM TUNNELING

A. General Model

The dynamics of a JJ is usually described by the RCSJ (resistively and capacitively shunted junction) model^{9,10}. The current flowing into the connecting leads comprises in addition to the Josephson current $I_J = I_c \sin \varphi$ (I_c denotes the critical current of the junction) a displacement current due to a shunting capacitance C and a dissipative component due to a frequency dependent shunting resistance R . For a complete description, the electromagnetic environment given by the measurement setup can be included in the model parameters. In our case, R will be

influenced by the environmental impedance while C can be regarded as solely determined by the plate capacitor geometry of the JJ itself. In any case, the bias current I is composed of

$$I = I_c \sin \varphi + \frac{1}{R} \frac{\Phi_0}{2\pi} \dot{\varphi} + C \frac{\Phi_0}{2\pi} \ddot{\varphi}, \quad (1)$$

where φ is the gauge-invariant phase difference across the junction and $\Phi_0 = h/2e$ is the magnetic flux quantum. The dynamics of φ as expressed by (1) is equally described by the well-studied Langevin equation

$$M\ddot{\varphi} + \eta M\dot{\varphi} + \frac{\partial U}{\partial \varphi} = \xi(t), \quad (2)$$

which describes a particle of mass $M = C(\Phi_0/2\pi)^2$ in a tilted washboard potential

$$U(\varphi) = E_J(1 - \cos \varphi - \gamma \varphi), \quad (3)$$

exposed to damping $\eta = 1/RC$ and under the influence of a fluctuating force $\xi(t)$. The strength of $\xi(t)$ is linked to temperature and damping by the fluctuation-dissipation theorem. Furthermore, $\gamma = I/I_c$ denotes the normalized bias current while $E_J = \Phi_0 I_c / 2\pi$ is called the Josephson coupling energy. For $\gamma < 1$, if thermal and quantum fluctuations are ignored, the particle is trapped behind a potential barrier

$$\Delta U = 2E_J \left(\sqrt{1 - \gamma^2} - \gamma \arccos \gamma \right), \quad (4)$$

and the JJ stays in the zero-voltage state. In the potential well, the phase oscillates with the bias current dependent plasma frequency

$$\omega_p = \omega_{p0} (1 - \gamma^2)^{1/4} = \sqrt{\frac{2\pi I_c}{\Phi_0 C}} (1 - \gamma^2)^{1/4}. \quad (5)$$

To complete the list of important system parameters given in this section, we introduce the quality factor

$$Q = \omega_p / \eta = \omega_p RC, \quad (6)$$

which is conventionally used to quantify the damping in the JJ.

At finite temperatures, the thermal energy $k_B T$ (k_B being Boltzmann's constant) described by $\xi(t)$ in (2) can lift the phase particle over the potential barrier before the critical current $\gamma = 1$ is reached, so that the particle will start rolling down the potential. This is called premature switching and the observed maximal supercurrent $I_{sw} < I_c$ is called the switching current. When the phase particle is rolling, the JJ is in the voltage state, since a voltage drop according to $\dot{\varphi} = (2\pi/\Phi_0)V$ is observed. The thermal escape from the potential well occurs with a rate^{11,12}

$$\Gamma_{th} = a_t \frac{\omega_p}{2\pi} \exp\left(-\frac{\Delta U}{k_B T}\right), \quad (7)$$

where a_t is a temperature and damping dependent prefactor, which will be discussed in more detail in Sec. II C.

For $T \rightarrow 0$, where $\Gamma_{th} \rightarrow 0$, premature switching will still be present due to quantum tunneling through the potential barrier. As the phase difference over the JJ is a macroscopic variable, this phenomenon is often referred to as "Macroscopic Quantum Tunneling" (MQT). This means that by measuring the switching events of a JJ for decreasing temperature, one will see a temperature dependent behavior (dominated by the Arrhenius factor $\exp(-\Delta U/k_B T)$ in (7)) until a crossover to the quantum regime is observed. The crossover temperature T_{cr} is approximately given by^{7,13}

$$T_{cr} = \frac{\hbar \omega_p}{2\pi k_B} = \frac{\hbar \omega_{p0}}{2\pi k_B} \cdot (1 - \gamma^2)^{1/4}, \quad (8)$$

where \hbar is Planck's constant. We can write the quantum tunneling rate for temperatures well below crossover as^{7,14-16}

$$\Gamma_q = a_q \frac{\omega_p}{2\pi} \exp(-B), \quad (9)$$

where $a_q = \sqrt{864\pi \Delta U / \hbar \omega_p} \exp(1.430/Q)$ and $B = (36\Delta U / 5\hbar \omega_p)(1 + 0.87/Q)$. In the limit of large Q , the escape rate is expected to approach the temperature independent expression (9) quickly^{15,17} once the temperature falls below T_{cr} . The rates in (7) and (9) are functions of the normalized bias current γ via (4) and (5). The crossover to the quantum regime can be nicely visualized by measuring the bias current dependence of the escape rate $\Gamma(I)$ for a sequence of falling temperatures. The data are then described over the whole temperature range by the thermal rate (7) with the temperature as a fitting parameter. In this way, one obtains a virtual "escape temperature" T_{esc} , which can be compared to the actual bath temperature T . In the thermal regime, one should obtain $T_{esc} = T$ while in the quantum regime, one should get $T_{esc} = T_{cr} = \text{const.}$

B. Influence of JJ Size on MQT

The crucial element of a Nb-based Josephson junction as employed in this work is the Nb/Al-AlO_x/Nb trilayer. For a JJ, $I_c = j_c \cdot A$ and $C = c \cdot A$, where the critical current density j_c and the specific capacitance c are constant for a given trilayer and A is the area of the junction. Hence, by reformulating (5), we find that $\omega_{p0} = \sqrt{2\pi j_c / \Phi_0 c}$, meaning that for JJs fabricated with the same trilayer, the plasma frequency does not depend on their size. So at first sight, the crossover temperature (8) should also be independent of the JJ size. In reality, however, the problem is more subtle, as one needs to take into account at which normalized bias current γ_{cr} the quantum tunneling rate (9) becomes significant. Since the height of the potential barrier $\Delta U \propto E_J \propto A$ is proportional to the JJ size, a significant tunneling rate should be reached at different γ_{cr} values for junctions of

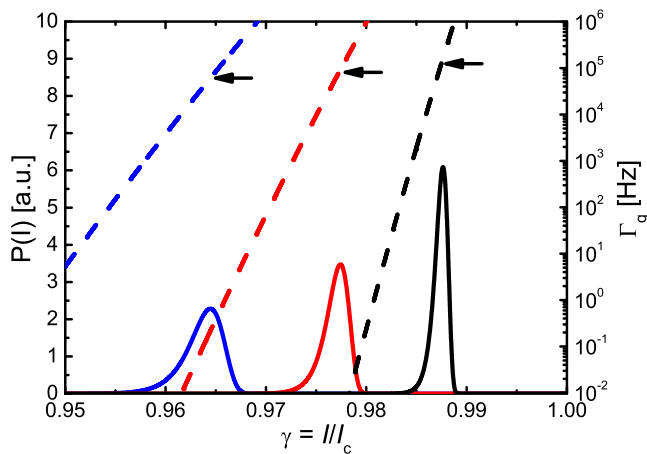


FIG. 1. Theoretically calculated switching current distributions $P(I)$ (solid curves) and quantum tunneling rates Γ_q (dashed curves) for samples B1 (left) to B3 (right) having different diameters d (for parameters see Tab. I). The difference in γ_{cr} (maximum position of $P(I)$), where quantum tunneling leads to escape from the potential well, is significant. The tunneling rates at these points (marked by arrows) are of the order of ≈ 100 kHz for all samples.

different size. These points can be estimated by theoretically calculating (9) and converting it into a switching current histogram, as it would be observed in a real experiment. The probability distributions of switching currents $P(\gamma)$ can be obtained from the quantum rate by equating¹⁸

$$P(\gamma) = \Gamma_q \left(\frac{d\gamma}{dt} \right)^{-1} \left(1 - \int_0^I P(u) du \right), \quad (10)$$

where $d\gamma/dt = (1/I_c) \cdot (dI/dt)$ is a constant for the linear current ramp chosen in our experiment. For the parameters of the junctions investigated in this work (see Tab. I), the switching current distributions $P(\gamma)$ were determined with a quality factor of $Q = 100$ and a current ramp rate of 100 Hz, according to our experiments (see below). They are shown in Fig. 1, where it can be seen that the γ_{cr} values (the positions of the maxima of the distributions) significantly and systematically increase with the junction size. Evaluation of the $\Gamma_q(\gamma_{cr})$ values for the samples indicates that quantum tunneling will be experimentally observable at a rate of around $\Gamma_q \approx 10^5$ Hz.

Subsequently, the expected crossover temperature was calculated from (8) with $\gamma = \gamma_{cr}$. The sample parameters as well as the expected γ_{cr} and T_{cr} values are given in Table I. It can be seen that due to the term in parenthesis on the right hand side of (8), the crossover temperature systematically decreases for increasing junction size. The change in T_{cr} is large enough to be observed experimentally. However, such a systematic study of the size-dependence of T_{cr} has never been carried out before.

TABLE I. Parameters of the investigated samples and calculated γ_{cr} and T_{cr} values. The critical current density accounts for $j_c \approx 650$ A/cm² while the specific capacitance of $c = 55$ fF/ μm^2 was recently determined by the measurement of Fiske steps on a trilayer prepared in our lab under identical conditions. Parasitic capacitances due to idle regions next to the JJs have been taken into account for all calculations in this article. For the calculation of T_{cr} , the actual measured critical currents were used.

Sample	Diameter d (μm)	γ_{cr}	T_{cr} (mK)
B1	1.9	0.965	371
B2	2.55	0.977	323
B3	3.6	0.988	291
B4	3.8	0.988	277

C. Influence of Damping on MQT

The quality parameter Q is frequently employed to describe the strength of the hysteresis in the current-voltage characteristics of a JJ. In this case, one often takes $Q = \omega_p R_{sg} C$ with R_{sg} being the subgap resistance of the junction. Here, Q is size-independent, as $R_{sg} \propto 1/A$ and $C \propto A$. In the context of MQT, however, the dynamics takes place at a frequency of ω_p , so that a complex impedance at that frequency $Z(\omega_p)$ has to be considered. For an MQT experiment, where the phase and not the charge is the well-defined quantum variable, the admittance $Y(\omega_p)$ will be responsible for damping¹⁹, so that R in (6) will be given by $R = 1/\text{Re}(Y)$.

If the junction was an isolated system, the value of R in the context of MQT would be determined by the intrinsic damping in the zero-voltage state. The value which is typically taken as a measure for this is the maximal subgap resistance $R_{sg,max}$, which is simply the maximal resistance value which can be extracted from the nonlinear subgap branch of the current-voltage characteristics^{20,21}. In most experiments however, the electromagnetic environment of the JJ can be assumed to have an impedance that is real and accounts for $Z_0 \approx 100 \Omega$, corresponding to typical transmission lines⁷. As furthermore $Z_0 \ll R_{sg,max}$ and both contributions are in parallel (see Fig. 2a), we can simply write $Q = \omega_p Z_0 C$ in this case.

Evidently, for junctions having a small capacitance (as in our experiment), the quality factor $Q = \omega_p Z_0 C$ will be limited to $Q \lesssim 10$ and additionally depend on the JJ size like $C \propto A$. As we want to investigate the pure influence of the JJ size on MQT, we would like to obtain very low damping as well as similar damping for all investigated junctions. In the implementation of phase qubits, current biased Josephson junctions have been inductively decoupled from their environment by the use of circuits containing lumped element inductors and an additional filter junction³. In order to keep our circuits simple, we attempted to reach a similar decoupling by only using on-chip lumped element inductors right in front of the

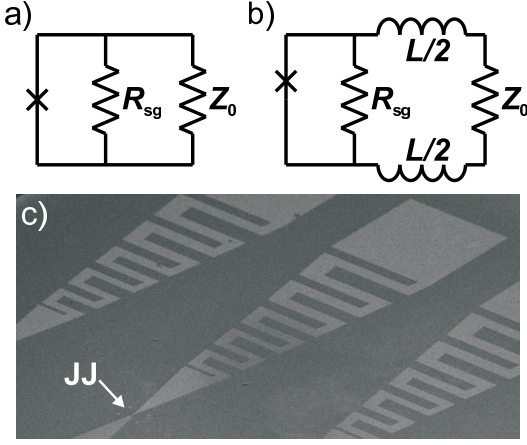


FIG. 2. a) Typical impedance environment for switching experiments in a JJ. As $Z_0 \ll R_{sg}$, the junction sees the impedance Z_0 at the plasma frequency. b) Lumped element inductors L can be used to decouple the JJ from the line impedance Z_0 , as discussed in the text. c) SEM micrograph of the electrode design used for the investigated junctions.

JJs (see Fig. 2b). This setup leads to an admittance

$$Y = 1/R_{sg,max} + 1/(Z_0 + i\omega L). \quad (11)$$

As for (11), we find $\text{Re}(Y) \rightarrow 1/R_{sg,max}$ in the limit $\omega L \rightarrow \infty$, big enough lumped element inductances should decouple the JJ from the Z_0 environment and result in a high intrinsic quality factor $Q = \omega_p R_{sg,max} C$ even for switching experiments. Although it might be difficult to reach this limit in a real experiment, decoupling inductors should definitively help to increase the quality factor and move towards a JJ-size independent damping.

The damping in the JJ influences the thermal escape rate (7) via the prefactor $a_t < 1$, which has been calculated for the first time by Kramers in 1940¹¹. In the limiting case $Q \rightarrow 0$ (moderate to high damping), he found:

$$a_t = \alpha_{KMD} = \sqrt{1 + \left(\frac{1}{2Q}\right)^2} - \frac{1}{2Q},$$

while in the opposite limit $Q \rightarrow \infty$ (very low damping limit), he found:

$$a_t = \alpha_{KLD} = \frac{36\Delta U}{5Qk_B T}.$$

More recently, Büttiker, Harris and Landauer²² extended the very low damping limit to the regime of low to moderate damping finding the expression²³

$$a_t = \frac{4}{(\sqrt{1 + 4/\alpha_{KLD}} + 1)^2}. \quad (12)$$

Additionally, damping reduces the crossover temperature according to^{12,24}

$$T_{cr,Q} = \frac{\hbar\omega_p}{2\pi k_B} \cdot \alpha_{KMD}. \quad (13)$$

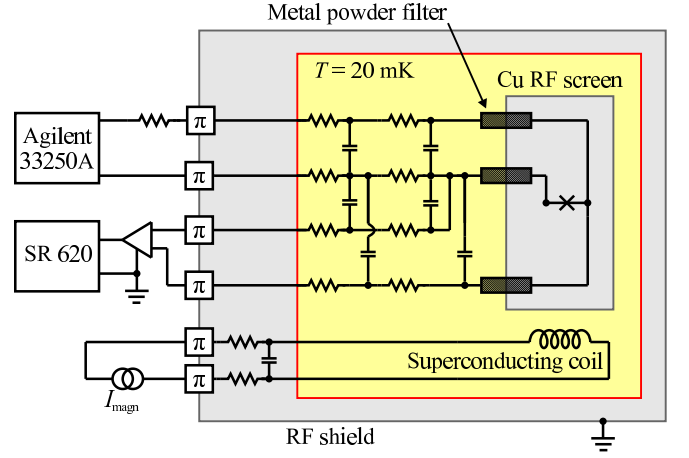


FIG. 3. Schematic overview of the measurement system. The superconducting coil and the sample are inside a magnetic shield consisting of three nested cylindrical beakers, the middle one made from Pb, the two remaining ones from *Cryo-erm*. Furthermore, the entire dilution refrigerator is placed inside a μ -metal shield at room temperature. The π -symbols denote commercial π -filters.

A possible way to determine the quality factor Q for such quantum measurements is to extract it from spectroscopy data⁷. Unfortunately, for samples with such a high critical current density as used in our experiments described here, this turns out to be experimentally very hard. Hence, we will limit the analysis of the damping in our experiments to the MQT measurements. However, other groups have found a good agreement between the Q values determined by spectroscopy and by MQT^{7,8} and we hope to observe such a major increase in Q due to the decoupling inductors that minor uncertainties in Q should not play a role.

III. SETUP AND PROCEDURE OF MEASUREMENT

All samples were fabricated by a combined photolithography / electron beam lithography process based on Nb/Al-AlO_x/Nb trilayers. The trilayer deposition was optimized carefully in order to obtain stress-free Nb films. For the definition of the Josephson junctions, an Al hard mask is created employing electron beam lithography. This hard mask acts as an ideal etch stopper during the JJ patterning with reactive-ion-etching. Furthermore, it allows the usage of anodic oxidation even for small junctions, which would not be possible if a resist mask was used. After the anodic oxidation, the Al hard mask is removed by a wet etching process. Details of this Al hard mask technique and the entire fabrication process are discussed elsewhere²⁵.

Our measurement setup can be seen in Fig. 3. Special care has been taken in design of the filtering stages in order to reach a low-noise measurement environment.

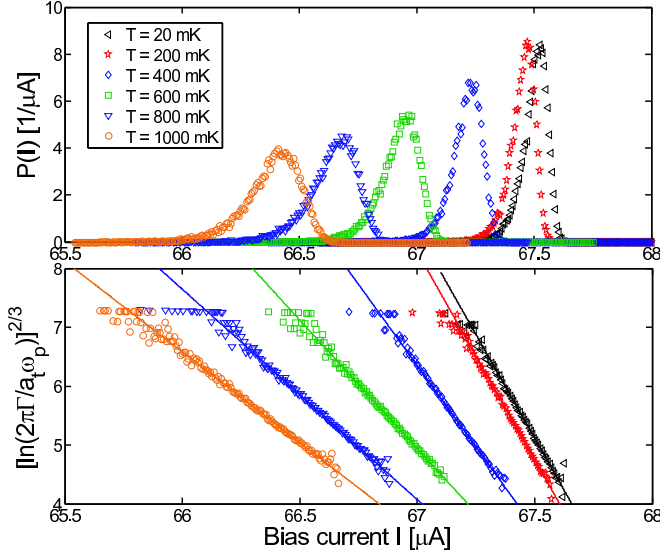


FIG. 4. Top: The measured switching current histograms for sample B3 for selected temperatures. For increasing T , the switching currents decrease and the histograms broaden. Bottom: The plot obtained by applying (15) for the same sample. The fits allow to extract T_{esc} as well as I_c .

The goal of the measurement is to determine the escape rate Γ . In order to do so, we have measured the probability distribution $P(I)$ of switching currents. This was done by ramping up the bias current with a constant rate $\dot{I} = dI/dt$ and measuring the time t_{sw} between $I = 0$ and the switching to the voltage state with a Stanford Research 620 Counter, so that $I_{\text{sw}} = \dot{I} \cdot t_{\text{sw}}$ could be calculated. An Agilent 33250A waveform generator was used to create a sawtooth voltage signal with a frequency of 100 Hz, which was converted into the bias current by a resistor of 47 k Ω . In this way, for each temperature, I_{sw} could be measured repeatedly. After doing so 20,000 times, the switching current histograms $P(I)$ with a certain channel width ΔI were attained as shown in the upper part of Fig. 4. These histograms were then used to reconstruct the escape rate out of the potential well as a function of the bias current by employing^{7,18}

$$\Gamma(I) = \frac{\dot{I}}{\Delta I} \ln \frac{\sum_{i \geq I} P(i)}{\sum_{i \geq I + \Delta I} P(i)}. \quad (14)$$

With Γ at hand, we could now determine the escape temperature T_{esc} by employing (7). In order to be able to rearrange this formula, we approximate the potential barrier in the limit $\gamma \rightarrow 1$ as $\Delta U = 4\sqrt{2}/3 \cdot E_J \cdot (1 - \gamma)^{3/2}$, so that we find

$$\left(\ln \frac{2\pi\Gamma(I)}{a_t(I)\omega_p(I)} \right)^{2/3} = \left(\frac{4\sqrt{2}E_J}{3k_B T_{\text{esc}}} \right)^{2/3} \frac{I_c - I}{I_c}. \quad (15)$$

Hence, by plotting the left side of (15) over the bias current I , we should obtain straight lines (see bottom part of Fig. 4). Consequently, we can extract the theoretical

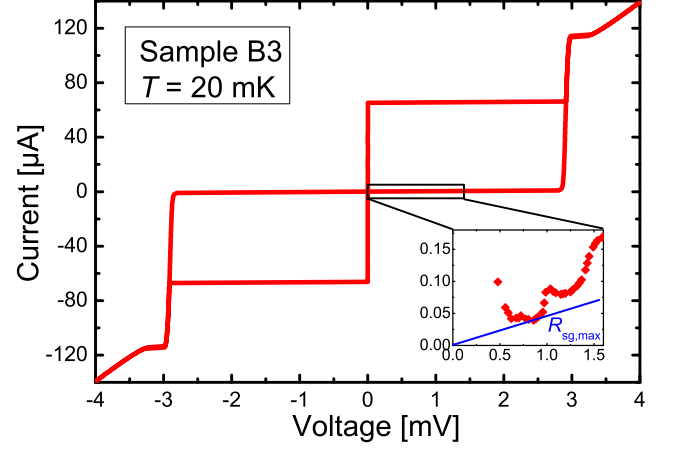


FIG. 5. Characterization of sample B3. The IV curve shows the high quality regarding the $I_c R_N$ ratio as well as low subgap currents. The inset shows a magnification of the subgap branch achieved by a voltage bias. The blue line illustrates how the value for $R_{\text{sg,max}}$ was determined. The fact that the current rises for decreasing voltage at $V \approx 0.5$ V is due to the fact that the junction jumps back to a supercurrent $I \neq 0$ for $V = 0$.

critical current I_c in the absence of any fluctuations as well as the escape temperature T_{esc} by applying a linear fit with slope a and offset b . We then find

$$I_c = -\frac{b}{a} \quad \text{and} \quad T_{\text{esc}} = -\frac{4\sqrt{2}\Phi_0}{6\pi k_B a \sqrt{b}}.$$

Since I_c enters (15) via E_J and ω_p , this fitting procedure has to be iteratively repeated until the value of I_c converges. So strictly speaking, this procedure involves two fitting parameters, namely T_{esc} and I_c . However, it turns out that I_c is temperature independent within the expected experimental uncertainty (for all our measurements, the fit values of I_c vary over the entire temperature range with a standard deviation of only around 0.09 %). Furthermore, the found I_c values agree very well with the expected ones from the critical current density j_c of the trilayer and the junction geometry. Altogether, it can be said that the results for the main fitting parameter T_{esc} should be very reliable.

IV. SAMPLE CHARACTERIZATION

The JJs were circular in shape and their geometries are given in Table I. In order to characterize the samples, IV curves with current bias as well as IV curves with voltage bias were recorded (an example can be seen in Fig. 5). The quality parameters for all samples are given in Table II and indicate a very high quality. In the voltage bias measurements, two major current drops at voltages $2\Delta/2$ and $2\Delta/3$ could be seen and attributed to Andreev reflections²⁶. Below $2\Delta/3$, we were able to extract values

of the maximal subgap resistance $R_{\text{sg,max}}$ as illustrated by the blue line in Fig. 5.

TABLE II. Experimentally determined parameters for all investigated JJs. The theoretical critical currents I_c were extracted from the MQT measurements. The $R_{\text{sg,max}}$ values were obtained as shown in the inset of Fig. 5a.

Sample	I_c (μA)	V_{gap} (mV)	$I_c R_N$ (mV)	$R_{\text{sg,max}}$ (k Ω)
B-1	19.1	2.88	1.75	54.0
B-2	31.9	2.88	1.86	73.0
B-3	68.1	2.92	1.93	21.1
B-4	70.8	2.90	1.91	31.5

V. RESULTS AND DISCUSSION

A. Damping in the Junctions

In order to decouple the JJs from their environmental impedance, the electrodes leading to the junctions were realized as lumped element inductors, as can be seen in Fig. 2c. This design was based on the layout that we recently used to successfully realize lumped element inductors for LC circuits in the GHz frequency range²⁷. Furthermore, simulations with Sonnet²⁸ confirmed that the meandered electrodes indeed act as lumped element inductors at the relevant frequencies $\omega_p(\gamma_{\text{cr}})$. The complex simulation with Sonnet gives an inductance of $L/2 \approx 1.65$ nH (for one electrode) while the much simpler analysis with FastHenry²⁹ yields $L/2 \approx 1.8$ nH.

For each sample, the data were analyzed using a number of different Q values in order to see if we could determine the experimentally observed damping. This was done by calculating the deviation of T_{esc} from the bath temperature T in the thermal regime:

$$\Delta T^2 = \sum_{T > 500 \text{ mK}} (T_{\text{esc}} - T)^2 \quad (16)$$

and finding its minimum value regarding Q . The corresponding values were then used for the sample analysis. It can be seen in Fig. 6 that the points of experimentally observed damping could be clearly identified. The evaluated Q values are given in Table III.

In a preliminary experiment, we investigated MQT in a junction with a diameter of $d = 1.9$ μm , a critical current of $I_c \approx 12$ μA and low-inductance electrodes, which were simple wide lines and can be imagined as the envelope of the electrodes in Fig. 2c. We carried out a similar analysis to determine the damping and obtained a quality factor of $Q = 4$. Subsequently, we evaluated (6) and calculated an impedance of $R = 99.8$ Ω , which is very close to the expected value of $Z_0 \approx 100$ Ω for typical transmission lines⁷. This means that with this simple preliminary design, the junction was in no way decoupled from the electromagnetic environment.

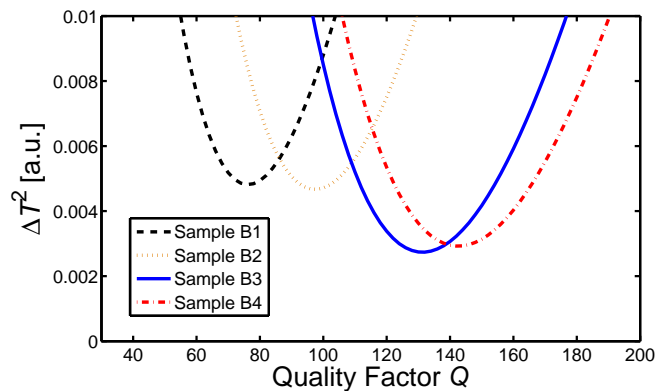


FIG. 6. Determination of the experimentally observed quality factor Q for all samples. The curves are minimal when the determined T_{esc} values deviate the least from the corresponding bath temperatures T in the thermal regime $T > 500$ mK.

The Q values obtained by using inductive electrodes (see Tab. III), however, show that we have drastically increased the quality factors with respect to the preliminary measurement. If we calculate the R values using (6), we find that they are clearly above the typical line impedance of $Z_0 \approx 100$ Ω as well as the vacuum impedance of 377 Ω , which shows that we were indeed able to inductively decouple the JJ from its usual impedance environment. As expected, the determined R values are still clearly below the subgap resistance $R_{\text{sg,max}}$, indicating that we have not reached the limit $\omega L \rightarrow \infty$. Instead, we are in the intermediate regime $Z_0 \ll R \ll R_{\text{sg,max}}$, leading to the fact that Q still exhibits a slight dependence on the JJ size (see Table III). However, all JJs are in the low-damping regime, so that no influence of damping on the results should be present and differences in the experimental results should indeed be due to the JJ size. This can be seen by the fact that the damping related correction in T_{cr} according to equation (13) is smaller than 1 % for all experimentally observed Q values. Altogether, we can state that we will be able to carry out our investigation of the size dependence of MQT with very low and nearly size-independent damping.

In addition to the rather qualitative considerations above, we performed a quantitative analysis employing

TABLE III. The experimentally determined values characterizing the damping for all samples. The L_{calc} values were determined from Q , the values given in Table II and equation (11). They are in good agreement with the design value of $L \approx 3.3$ nH.

Sample	Q	R (Ω)	L_{calc} (nH)
B-1	76	1571	1.33
B-2	98	1327	1.39
B-3	132	1015	1.36
B-4	143	1041	1.43

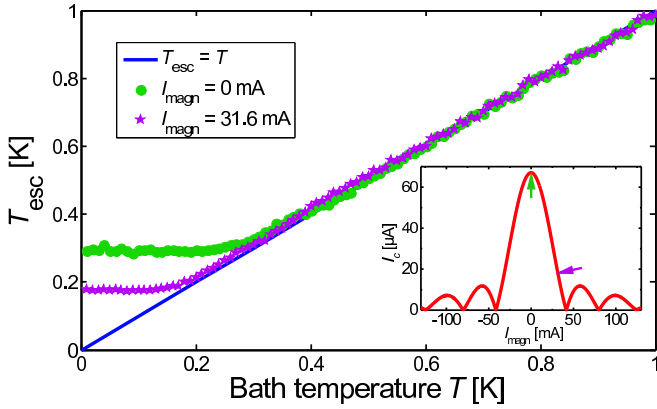


FIG. 7. Calculated escape temperatures for sample B3 with and without an applied magnetic field. The inset shows the $I_c(\Phi)$ modulation of this junction; the arrows indicate where the MQT data was obtained. For $I_{\text{magn}} = 31.6$ mA, a clear reduction of the observed crossover temperature T_{cr} is observed.

equation (11). If we use $\omega = \omega_p(\gamma_{\text{cr}})$, take $R_{\text{sg,max}}$ from Table II and assume that $Z_0 = 100\Omega$, we can calculate the decoupling inductance L_{calc} for all samples. The values, given in Table III, are a factor of around 2.3 – 2.5 smaller than the simulation value of $L \approx 3.3$ nH, but of the right order of magnitude. For such a complex system, this is a surprisingly good agreement between simulation and theory on the one side and experimentally determined values on the other side. In summary, we conclude that we have successfully demonstrated that decoupling of the Josephson junction from its environment is also possible using only lumped element inductors.

B. Crossover to the Quantum Regime

We now turn to the investigation of the crossover point from the thermal to the quantum regime and the influence of JJ size on it. As can be seen in Table I, we expect a clear reduction of T_{cr} with increasing JJ size. However, an experimental observation of lower crossover temperatures for smaller JJs having smaller critical currents could simply be due to current noise in our measurement setup. In order to exclude this, we artificially reduced the critical current of sample B3 by applying a magnetic field in parallel to the junction area. While unwanted noise should now lead to an increase in the observed T_{cr} , the physical expectation is a significantly reduced T_{cr} due to the lower plasma frequency according to (8). The result of this measurement can be seen in Fig. 7 and Table IV. We found an agreement between calculated and observed crossover temperature down to $T_{\text{cr}} \approx 140$ mK, which was the lowest temperature we examined. Hence, it is clear that we have a measurement setup exhibiting low noise, where the electronic temperature is indeed equal to the bath temperature. The lowest investigated temperature of 140 mK is clearly below any temperature needed for

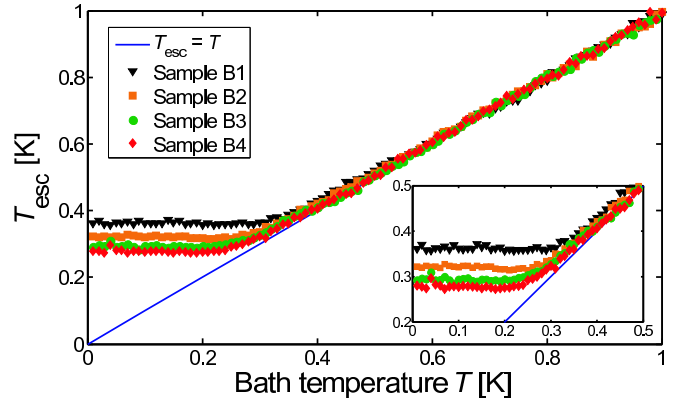


FIG. 8. Calculated escape temperatures for all samples. The crossover to the quantum regime is very clear in each measurement. The inset shows a magnification of the quantum regime. The reduction of the crossover temperature T_{cr} with increasing JJ size is clearly visible.

the comparison of the JJs of different sizes with each other.

Finally, we measured the switching histograms for the four JJs of different sizes and evaluated the escape temperature T_{esc} and the theoretical critical current I_c . This allowed us to determine the crossover temperature T_{cr} and the normalized crossover current $\gamma_{\text{cr}} = I_{\text{sw,cr}}/I_c$. We indeed found a clear dependence of the crossover temperature on the JJ size as can be seen in Fig. 8. To compare the experimental γ_{cr} and T_{cr} values with the ones expected by theory, we now performed the theoretical calculation described above using the experimentally determined Q values and equation (13). All experimentally determined values are in excellent agreement with theory, as can be seen in Table IV.

TABLE IV. The experimentally determined values characterizing the crossover from the thermal to the quantum regime in comparison with the theoretical expectations for all measurements.

Sample	$I_c(\Phi)/I_c(0)$	$\gamma_{\text{cr,theo}}$	$\gamma_{\text{cr,exp}}$	$T_{\text{cr},Q,\text{theo}}$ (mK)	$T_{\text{cr,exp}}$ (mK)
B-1	1	0.965	0.970	368	362
B-2	1	0.977	0.981	322	321
B-3	1	0.988	0.990	290	294
B-3	0.52	0.984	0.987	223	236
B-3	0.27	0.979	0.983	172	176
B-3	0.13	0.973	0.975	129	147
B-4	1	0.988	0.990	276	278

VI. CONCLUSIONS

We have carried out systematic Macroscopic Quantum Tunneling (MQT) experiments with varying Josephson junction area. Our samples were fabricated on the same

chip. Thorough characterization before the actual quantum measurements revealed that the junctions exhibit a very high quality. We showed that we could significantly decrease the damping at frequencies relevant for MQT by using lumped element inductors, which allowed us to perform our study in the low damping limit. The crossover from the thermal to the quantum regime was found to have a clear and systematic dependence on junction size,

which is in perfect agreement with theory.

ACKNOWLEDGMENTS

This work was partly supported by the DFG Center for Functional Nanostructures, project number B1.5. We would like to thank A. V. Ustinov for useful discussions.

-
- * Roland.Schaefer@kit.edu
- ¹ Y. Nakamura, Y. A. Pashkin, and J. S. Tsai, *Nature*, **398**, 786 (1999).
 - ² J. R. Friedman, V. Patel, W. Chen, S. K. Tolpygo, and J. E. Lukens, *Nature*, **406**, 43 (2000).
 - ³ J. M. Martinis, S. Nam, and J. Aumentado, *Physical Review Letters*, **89**, 117901 (2002).
 - ⁴ D. Vion, A. Aassime, A. Cottet, P. Joyez, H. Pothier, C. Urbina, D. Esteve, and M. H. Devoret, *Science*, **296**, 886 (2002).
 - ⁵ I. Chiorescu, Y. Nakamura, C. J. P. M. Harmans, and J. E. Mooij, *Science*, **299**, 1869 (2003).
 - ⁶ R. F. Voss and R. A. Webb, *Physical Review Letters*, **47**, 265 (1981).
 - ⁷ J. M. Martinis, M. H. Devoret, and J. Clarke, *Physical Review B*, **35**, 4683 (1987).
 - ⁸ A. Wallraff, A. Lukashenko, C. Coqui, A. Kemp, T. Duty, and A. V. Ustinov, *Review of Scientific Instruments*, **74**, 3740 (2003).
 - ⁹ W. C. Stewart, *Applied Physics Letters*, **12**, 277 (1968).
 - ¹⁰ D. E. McCumber, *Journal of Applied Physics*, **39**, 3113 (1968).
 - ¹¹ H. A. Kramers, *Physica (Utrecht)*, **7**, 284 (1940).
 - ¹² P. Hänggi, P. Talkner, and M. Borkovec, *Reviews of Modern Physics*, **62**, 251 (1990).
 - ¹³ I. Affleck, *Physical Review Letters*, **46**, 388 (1981).
 - ¹⁴ A. O. Caldeira and A. J. Leggett, *Annals of Physics (N.Y.)*, **149**, 374 (1983).
 - ¹⁵ H. Grabert, P. Olschowski, and U. Weiss, *Physical Review B*, **36**, 1931 (1987).
 - ¹⁶ E. Freidkin, P. S. Riseborough, and P. Hänggi, *J. Phys. C: Solid State Phys.*, **21**, 1543 (1988).
 - ¹⁷ E. Freidkin, P. S. Riseborough, and P. Hänggi, *Z. Phys. B – Condensed Matter*, **64**, 237 (1986); **67**, 271 (1987).
 - ¹⁸ T. A. Fulton and L. N. Dunkleberger, *Physical Review B*, **9**, 4760 (1974).
 - ¹⁹ G. L. Ingold and Yu. V. Nazarov: *Charge Tunneling Rates in Ultrasmall Junctions*, “Single charge tunneling,” (Plenum Press, New York, 1992) p. 21, also available at arXiv:cond-mat/0508728v1.
 - ²⁰ F. P. Milliken, R. H. Koch, J. R. Kirtley, and J. R. Rozen, *Applied Physics Letters*, **85**, 5941 (2004).
 - ²¹ M. A. Gubrud, M. Ejrnaes, A. J. Berkley, R. C. R. Jr., I. Jin, J. R. Anderson, A. J. Dragt, C. J. Lobb, and F. C. Wellstood, *IEEE Transactions on Applied Superconductivity*, **11**, 1002 (2001).
 - ²² M. Büttiker, E. P. Harris, and R. Landauer, *Physical Review B*, **28**, 1268 (1983).
 - ²³ Equation (12) does not describe the turnover from low damping to high damping. This turnover problem has been addressed by several authors (see e.g. Hänggi *et al.*¹² and references therein). In general, more precise expressions agree with (12) in the parameter regime of our samples to within experimental resolution.
 - ²⁴ H. Grabert and U. Weiss, *Physical Review Letters*, **53**, 1787 (1984).
 - ²⁵ Ch. Kaiser *et al.*, submitted (2010), arXiv:1009.0167 [cond-mat].
 - ²⁶ G. B. Arnold, *Journal of Low Temperature Physics*, **68**, 1 (1987).
 - ²⁷ C. Kaiser, S. T. Skacel, S. Wünsch, R. Dolata, B. Mackrodt, A. Zorin, and M. Siegel, *Superconductor Science and Technology*, **23**, 075008 (2010).
 - ²⁸ Sonnet Software Inc., 1020, Seventh North Street, Suite 210, Liverpool, NY 13088, USA.
 - ²⁹ Fast Field Solvers, <http://www.fastfieldsolvers.com>.